

固溶时效处理对激光熔丝真空增材制造 Ti6Al4V 耐蚀性能的影响

丁雪萍^{1*}, 张祺², 马红林²

¹重庆理工大学材料科学与工程学院, 重庆 400054;

²中国科学院重庆绿色智能技术研究院智能增材制造技术与系统重庆市重点实验室, 重庆 400714

摘要 利用动电位极化曲线、电化学交流阻抗谱、X射线光电子能谱(XPS)和电子背散射衍射(EBSD)等测试方法研究了固溶时效处理对激光熔丝真空增材制造 Ti6Al4V 钛合金在质量分数为 3.5% 的 NaCl 溶液中的耐蚀性能的影响规律,其中固溶温度为 950 °C,时效温度分别为 500 °C 和 600 °C。研究表明,固溶时效处理后试样的腐蚀电流密度变小,腐蚀后试样表面生成的钝化膜中的高价态氧化物 TiO₂ 的含量增多,钝化膜更稳定,保护效果更好,耐蚀性能明显得到改善,其中 500 °C 时效试样的耐蚀性能最优,600 °C 时效试样次之。其原因是固溶时效处理后试样中的针状 α' 相减少,大角度晶界比例增加,导致耐蚀性能提高。此外,与 500 °C 时效试样相比,600 °C 时效试样中的 α 片层明显变厚,导致耐蚀性能变差。

关键词 激光技术; 激光真空增材制造; Ti6Al4V 合金; 固溶时效处理; 耐蚀性能

中图分类号 TG113 文献标志码 A

DOI: 10.3788/CJL230634

1 引言

Ti6Al4V 钛合金具有比强度高、耐蚀性能好、生物相容性优良等优点,被广泛应用于航空航天、生物医疗、海军工程等领域^[1]。针对复杂几何形状的钛合金零件的制造,传统铸造或锻造技术较难实现^[2]。近年来,金属增材制造技术快速蓬勃发展,为钛合金复杂零件制造提供了新的途径。其中,激光熔丝增材制造技术具有材料利用率高、熔覆效率高、绿色环保等诸多优点,被广泛应用于钛合金制造。针对钛合金激光熔丝增材制造,研究人员开展了大量研究。Gibson 等^[3]研究了多模式闭环控制对熔池大小的影响规律,Liu 等^[4]研究了工艺-成形-组织之间的关系,Fu 等^[5]研究了成形过程稳定性和微观组织特征,Sun 等^[6]利用数值模拟和实验测试方法研究了微观组织转变规律,Brandl 等^[7]研究了工艺参数和热处理工艺对力学性能的影响规律。现有研究大多集中在成形、组织、力学性能等方面。众所周知,钛合金常应用于耐蚀环境,亟须关注其耐蚀性能。值得注意的是,激光增材钛合金过程中极高的温度梯度和超快的冷却速率促使试样中形成大量针状 α' 相和少量 β 相,虽然 β 相是稳定相,耐蚀性能较好,但 α' 相是高能相,耐蚀性能较差。另外, α' 相和 β 相

之间存在的电位差会引起原电池腐蚀,再加上激光增材制造后零件中存在较大的残余拉应力,导致激光增材制造钛合金的耐蚀性能较差^[8]。

为增强激光增材制造钛合金的耐蚀性能,Ibrahim 等^[9]采用激光熔覆技术制备金属玻璃涂层,Yao 等^[10]采用微弧氧化技术制备 TiO₂ 涂层,Ramasamy 等^[11]采用等离子体喷涂技术制备羟基磷灰石涂层,利用制备的涂层作为物理屏障,通过物理隔离腐蚀介质与金属基体,进而增强耐蚀性能。但是外加涂层易出现孔隙/裂纹等缺陷,且涂层和基体的结合强度较低,易出现涂层开裂脱落等问题。为此,研究人员采用热处理调控微观组织,进而增强耐蚀性能。比如 Li 等^[12]研究发现,利用去应力退火可减少显微偏析,进而增强耐蚀性能。Ettfagh 等^[13]研究发现,退火后试样中的非平衡相 α' 相含量及残余应力降低,进而耐蚀性能增强。Xu 等^[14]研究发现,退火后 α' 和 β 两相界面面积减小,有利于增强耐蚀性能。现有研究表明,退火处理可明显增强激光增材制造钛合金的耐蚀性能,但是经过退火热处理后,零件强度和硬度有所降低^[15]。事实上,钛合金除了常用热处理进行除退火外,还可以用固溶时效进行处理。钛合金经固溶时效处理后不仅强度和硬度得到提升,同时其塑性和韧性得到改善。目前已有关于

收稿日期: 2023-03-21; 修回日期: 2023-04-13; 录用日期: 2023-05-30; 网络首发日期: 2023-07-04

基金项目: 重庆市自然科学基金面上项目(cstc2020jcyj-msxmX0505)、重庆市教委科学技术研究项目(KJQN202101148)、重庆理工大学科研创新团队培育计划(2023TDZ013)

通信作者: *dingxp@cqut.edu.cn

固溶时效处理对增材制造 Ti6Al4V 微观组织、力学性能和摩擦磨损行为等影响的研究^[16-18],但是其对耐蚀性能的影响研究尚未见报道。此外,目前钛合金激光熔丝增材制造多在氩气氛围下进行,研究发现,真空环境下的增材制造可显著减少零件中杂质的形成并避免氧化^[19-20],激光熔丝真空增材制造具有巨大潜力。目前固溶时效处理对激光熔丝真空增材制造钛合金耐蚀性能的影响规律尚不清晰,因此非常有必要进行深入研究。

本文研究了固溶时效处理对激光熔丝真空增材制造 Ti6Al4V 耐蚀性能的影响规律,首先通过动电位极化曲线、电化学阻抗谱、钝化膜特征的特征,研究了固溶时效处理对腐蚀行为的影响,然后对固溶时效处理前后试样的微观组织进行表征,研究了固溶时效处理前后试样的微观组织的演变规律,最后揭示了固溶时效处理对耐蚀性能产生影响的内在原因,为利用固溶时效处理调控增材制造钛合金的耐蚀性能提供了理论依据。

2 实验方法

利用激光熔丝真空增材制造实验系统(图 1)制备 Ti6Al4V 薄壁件试样。其中,激光系统由定制的 5 路波长为 808 nm 的半导体激光组成,每路激光的最大功

率为 60 W,聚焦光斑直径为 0.2 mm,与丝材间的夹角为 41°。5 路激光在基板上聚焦后形成的光斑形状为椭圆形,长轴和短轴长度分别为 0.8 mm 和 0.5 mm。在增材制造过程中,5 路激光聚焦在基板上,基板受热熔化形成熔池,将丝材竖直向下送入熔池,在熔池热量的作用下丝材熔化凝固,逐层制造试样。为了获得稳定的成形过程和良好表面成形,丝材的过渡形式为液桥过渡,增材制造薄壁件试样如图 2 所示。试样制备时激光功率为 180 W,送丝速度为 13 mm/s,扫描速度为 3 mm/s,层间停留时间为 10 s,真空压强为 5 Pa。对增材试样进行固溶时效热处理,已知 Ti6Al4V 钛合金的 $\alpha+\beta/\beta$ 相转变温度为 980~1000 °C,若在高于 β 相转变温度下进行固溶处理,晶粒尺寸会粗大,导致性能较差。因此,选择在 950 °C 下进行固溶处理。时效温度范围一般为 500~600 °C,选择 500 °C 和 600 °C 分别进行时效处理,具体固溶时效处理工艺如表 1 所示。为简化描述,未处理的原始试样标记为 AM,固溶时效处理试样分别标记为 SAT500 和 SAT600。

利用电子背散射衍射(EBSD)对增材试样和固溶时效试样的微观组织进行表征。测试前对试样进行研磨、机械抛光和电解抛光,其中电解液为高氯酸+甲醇(体积比为 1:9),抛光温度为 -35 °C,直流电压为 20 V,

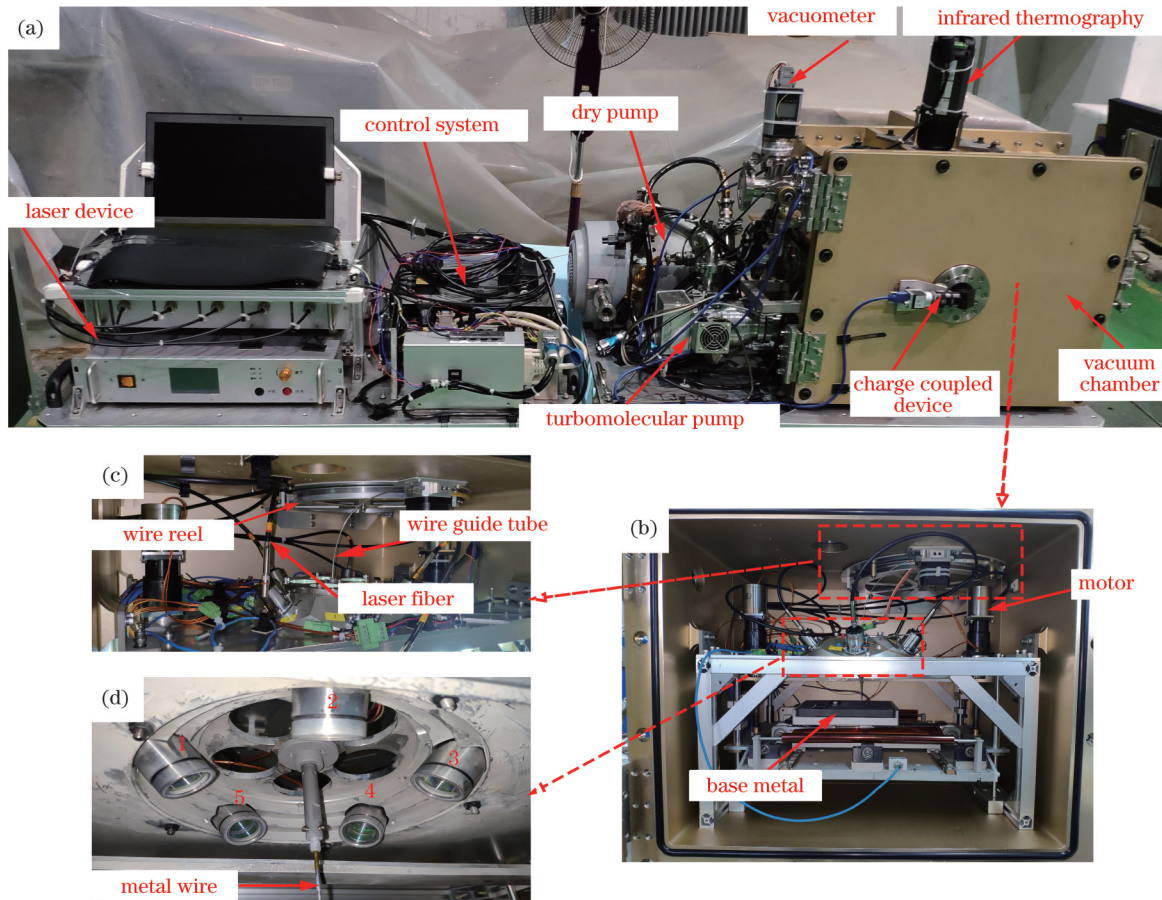


图 1 激光熔丝真空增材制造实验设备。(a)设备总体;(b)真空腔内设备;(c)送丝系统;(d)光丝排布方式

Fig. 1 Experimental equipment for laser wire vacuum additive manufacturing. (a) Overall equipment; (b) equipment in vacuum chamber; (c) wire feeding system; (d) laser and wire arrangement

抛光时间为 60 s。EBSD 测试后,利用 HKL Channel 5 软件对数据进行分析。

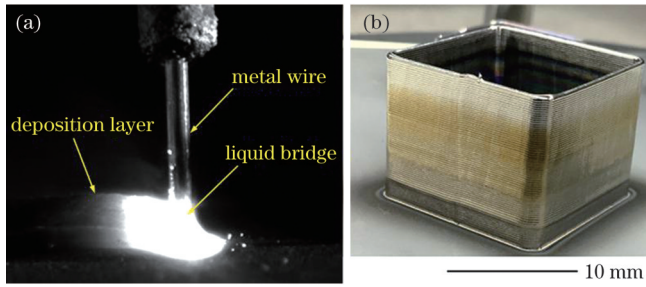


图 2 增材制造薄壁件。(a)液桥过渡图;(b)试样

Fig. 2 Additive manufacturing of thin-wall part. (a) Figure of liquid bridge transfer; (b) sample

表 1 固溶时效热处理的工艺参数

Sample	Temperature / °C	Time / h	Cooling method
SAT500	950	1	Air cooling
	500	4	Air cooling
SAT600	950	1	Air cooling
	600	4	Air cooling

对增材试样和固溶时效试样进行耐蚀性能表征,开展动电位极化曲线和电化学交流阻抗谱测试。测试系统选用电化学工作站,采用三电极系统,测试试样为工作电极,Ag/AgCl 电极为参比电极,Pt 片为对电极,测试溶液为质量分数为 3.5% 的 NaCl 溶液。电化学测试时,首先开展开路电位测试,待稳定后获得开路电位 (E_{ocp}),再分别开展电化学阻抗谱(EIS)测试和极化曲线测试。EIS 测试时,激励信号为幅值为 10 mV 的正弦波,频率为 $10^5 \sim 10^{-2}$ Hz。基于测试获得的 EIS 数据,利用 ZSimpWin 软件进行等效电路拟合。动电位极化曲线测试时,扫描速率为 0.1667 mV/s,扫描范围为 $-0.5 \sim 1.2$ V (相对于 E_{ocp})。采用 X 射线光电子能谱(XPS)分析试样表面形成的钝化膜的化学成分及元素价态组成。为去除表面污染,采用 Ar 离子刻蚀 10 nm 后再进行测试。测试后,所有元素峰值采用标准峰(C1s 峰,结合能为 248.8 eV)进行校准,之后利用 Thermo Advantage 软件进行拟合分析。

3 实验结果

3.1 腐蚀行为分析

图 3 为 AM、SAT500 和 SAT600 试样在质量分数为 3.5% 的 NaCl 溶液中的极化曲线。观察发现:AM 试样的阳极极化曲线无明显钝化区;SAT600 试样的阳极极化曲线可分为初级钝化区、过钝化溶解区、二次钝化区,说明钝化膜的稳定性较差;SAT500 试样的阳极极化曲线有明显钝化区,之后未发生溶解,说明有稳定的钝化膜形成。对比发现,SAT500 试样的

钝化电流密度 ($0.29 \mu\text{A}/\text{cm}^2$) 明显小于 SAT600 试样 ($199.52 \mu\text{A}/\text{cm}^2$),说明前者表面更易形成钝化膜。采用 Tafel 插值法拟合获得的自腐蚀电位 (E_{corr}) 和自腐蚀电流密度 (i_{corr}) 数值如表 2 所示,比较发现,AM 试样的 i_{corr} 数值分别是 SAT500 和 SAT600 试样的 74.83 倍和 7.39 倍,说明 SAT500 试样的耐蚀性最优,SAT600 试样次之,AM 试样最差。

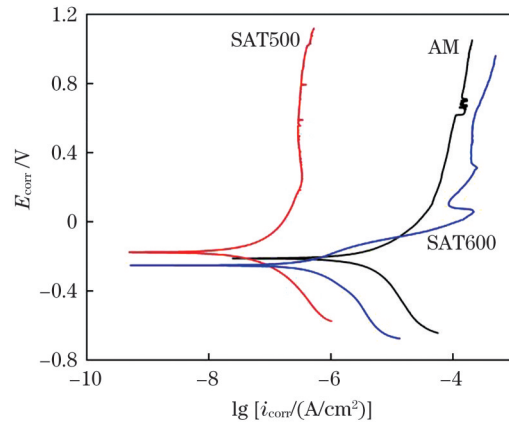


图 3 不同试样在质量分数为 3.5% 的 NaCl 溶液中的极化曲线
Fig. 3 Polarization curves of different samples in NaCl solution with mass fraction of 3.5%

表 2 不同试样的腐蚀电位和腐蚀电流密度值

Sample	E_{corr} / V	$i_{corr} / (\mu\text{A}/\text{cm}^2)$
AM	-0.213	2.595
SAT500	-0.175	0.035
SAT600	-0.238	0.351

图 4 为 AM、SAT500 和 SAT600 试样在质量分数为 3.5% 的 NaCl 溶液中的 EIS 测试结果,其中 Z_{im} 为阻抗虚部, Z_{Re} 为阻抗实部, Z_{mod} 为阻抗模值, f 为频率。结果显示,3 个试样均呈现容抗弧特征,SAT500 和 SAT600 试样的容抗弧半径大于 AM 试样,说明固溶时效处理后,腐蚀后的氧化膜厚度和均匀性得到提升。图 4(d) 为 EIS 等效电路模型,其中 R_s 为溶液电阻, R_f 为钝化膜电阻,CPE₁ 为钝化膜电容,CPE₂ 为双电层电容, R_{ct} 为电荷转移电阻。等效电路拟合结果如表 3 所示,其中 n_1 、 n_2 为弥散指数且 $0 < n_1 < 1$ 、 $0 < n_2 < 1$ 。观察发现,拟合数值和实验数值之间的差异程度 (χ^2) 很小,说明拟合结果与实验结果吻合良好。SAT500 和 SAT600 试样的 $R_f + R_{ct}$ 数值均大于 AM 试样,说明固溶时效热处理后试样的钝化膜的保护性能更好,进而耐蚀性能更优。综合极化曲线和 EIS 测试结果,发现固溶时效处理可显著改善激光熔丝真空增材 Ti6Al4V 的耐蚀性能,其中 SAT500 试样的耐蚀性能优于 SAT600 试样。

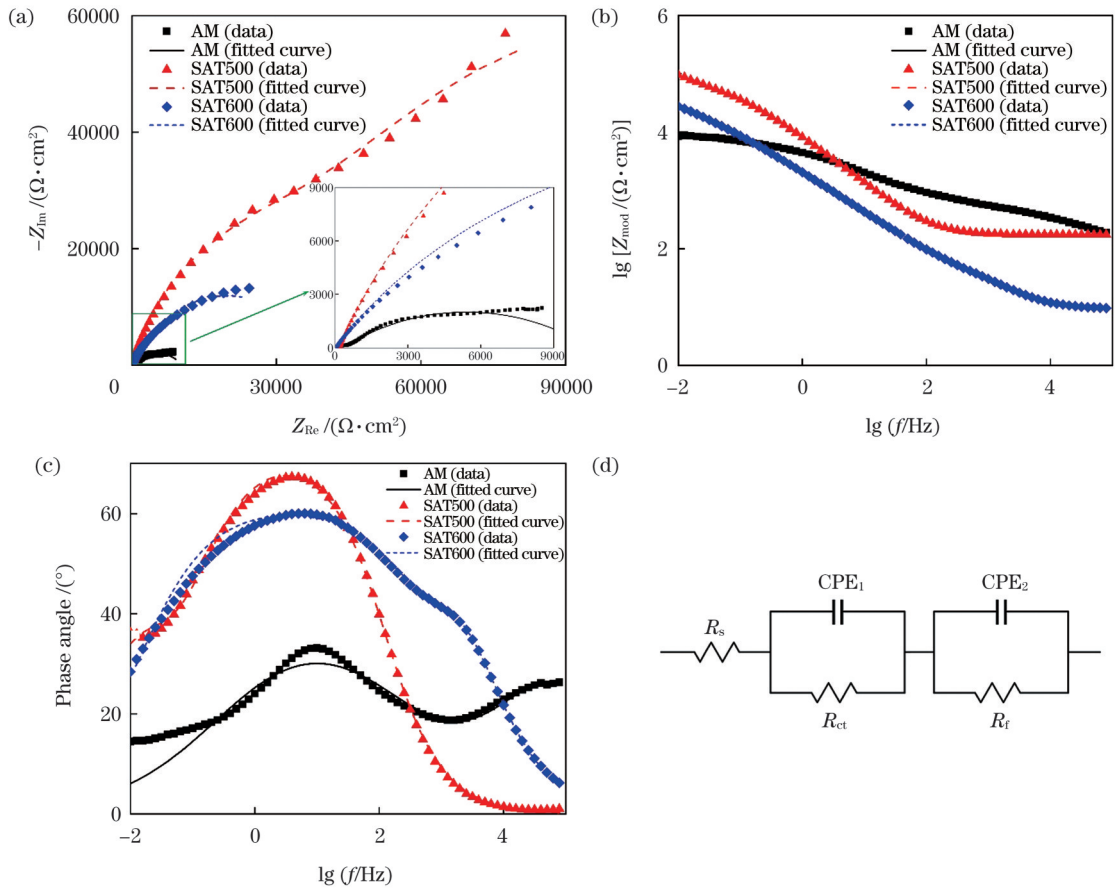


图 4 EIS 测试结果。(a)Nyquist 曲线；(b)(c)Bode 图；(d)等效电路模型

Fig. 4 EIS measurement results. (a) Nyquist plots; (b)(c) Bode plots; (d) equivalent circuit model

表 3 测试试样 EIS 等效电路拟合结果

Table 3 EIS parameters of equivalent circuit for test samples

Sample	$R_s / (\Omega \cdot \text{cm}^2)$	$\text{CPE}_1 / (\text{S} \cdot \text{s}^n / \text{cm}^2)$	n_1	$R_t / (10^4 \Omega \cdot \text{cm}^2)$	$\text{CPE}_2 / (\text{S} \cdot \text{s}^n / \text{cm}^2)$	n_2	$R_{ct} / (\Omega \cdot \text{cm}^2)$	χ^2
AM	181.6	2.999×10^{-5}	0.4834	2.341	9.797×10^{-7}	0.6234	758.300	3.024×10^{-3}
SAT500	172.4	3.323×10^{-5}	0.8093	4.08	1.223×10^{-4}	0.8303	1.461×10^5	3.046×10^{-4}
SAT600	91.02	1.357×10^{-4}	0.6867	3.975	3.042×10^{-5}	0.9199	9.328	7.323×10^{-4}

3.2 钝化膜成分分析

图 5 显示了 AM、SAT500 和 SAT600 试样表面形成的钝化膜的 XPS 全谱结果。可以看出,在钝化膜中主要有 O 1s、V 2p、Ti 2p、C 1s 和 Al 2p 峰。为了实现钝化膜成分的定量分析,开展了高分辨率 XPS 窄谱测试,结果如图 6 所示。由于 V 含量较少,峰强度较弱,故未进行 V 2p 窄谱分析。Ti 2p、O 1s、Al 2p 分峰结果如表 4 所示。观察发现, Ti 2p 光谱可分为三对独立峰,即 Ti^{4+} 、 Ti^{3+} 、Ti 峰,分别以 TiO_2 、 Ti_2O_3 、Ti 形式存在,其中 Ti^{4+} 峰强度明显强于 Ti^{3+} 和 Ti 峰,说明 Ti^{4+} 为主要成分。O 1s 光谱包含两个峰,即金属氧化物和羟基,羟基一般来自表面吸附的水分子。Al 2p 峰显示钝化膜中含有 Al_2O_3 。

图 7 显示了 AM、SAT500 和 SAT600 试样表面钝化膜中的 Ti 元素价态分布情况。观察发现,三个试样中 Ti^{4+} 含量均高于 Ti^{3+} 和金属 Ti,固溶时效处理后试

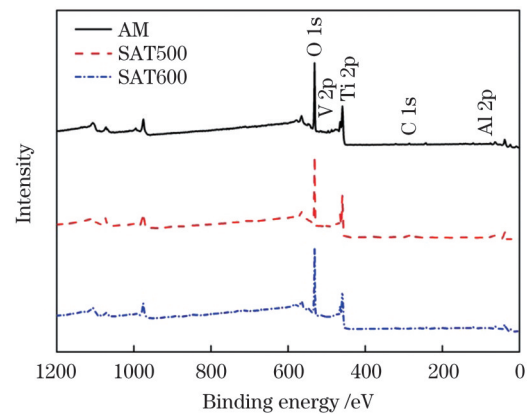


图 5 不同试样表面钝化膜的 XPS 全谱

Fig. 5 XPS full spectra of passive films formed on different sample surfaces

样中的 Ti^{4+} 含量呈现增加趋势。已有研究表明,高价态氧化物 TiO_2 具有更稳定和优异的保护效果^[21],因

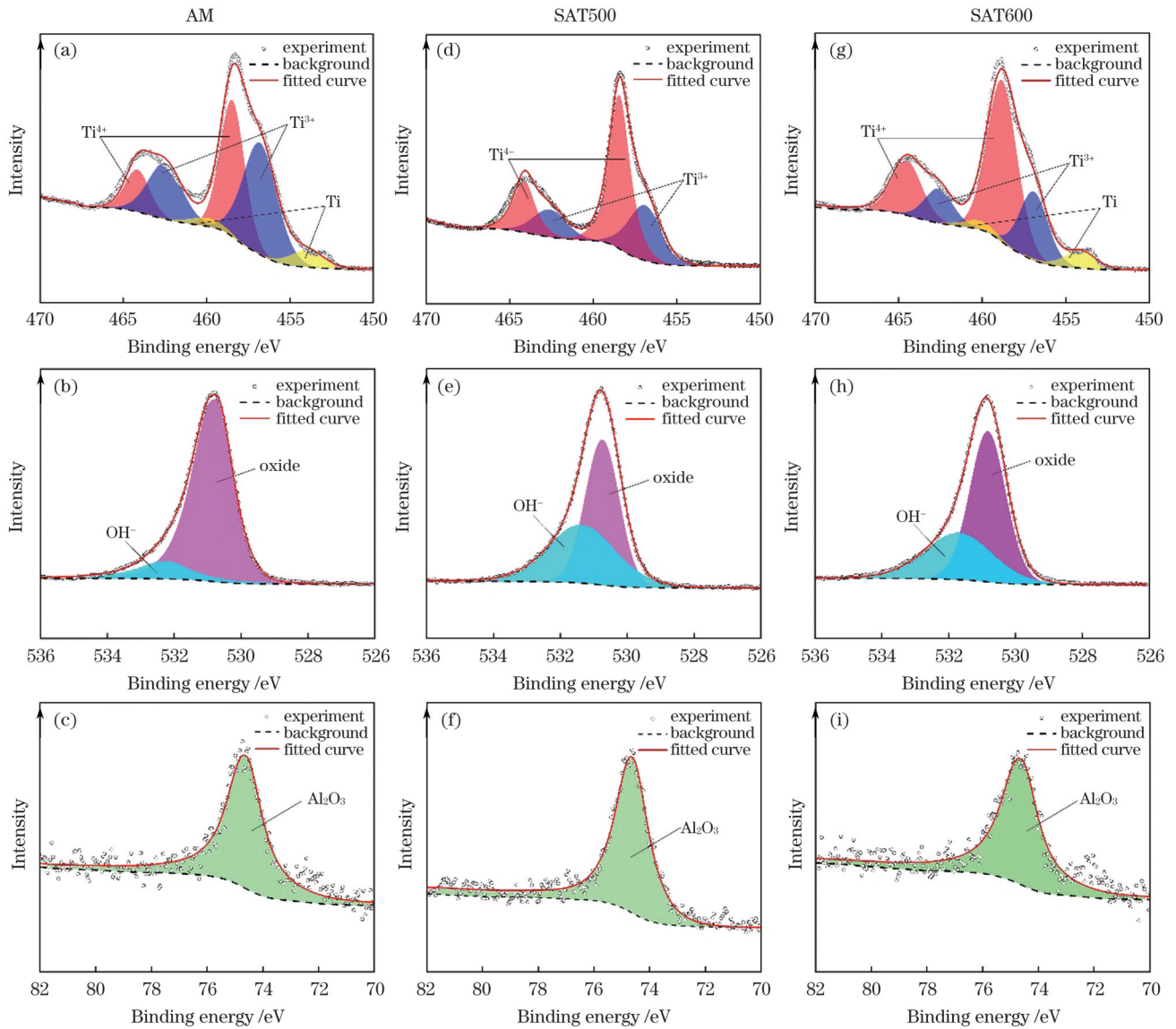


图 6 不同试样表面钝化膜的高分辨 XPS 光谱。(a)(d)(g) Ti 2p; (b)(e)(h) O 1s; (c)(f)(i) Al 2p

Fig. 6 High-resolution XPS spectra of passive films formed on different sample surfaces. (a)(d)(g) Ti 2p; (b)(e)(h) O 1s; (c)(f)(i) Al 2p

表 4 高分辨 XPS 光谱分峰拟合结果

Table 4 Results of peak fitting of high-resolution XPS spectra

Peak	Binding energy /eV			Chemical state
	AM	SAT500	SAT600	
Ti 2p	453.94	-	454.07	Ti
	456.8	456.90	456.90	Ti ₂ O ₃
	458.46	458.43	458.80	TiO ₂
	459.94	-	460.07	Ti
	462.5	462.60	462.60	Ti ₂ O ₃
	464.16	464.13	464.50	TiO ₂
O 1s	530.73	530.61	530.71	Metal oxides
	532.39	531.52	531.74	OH ⁻
Al 2p	74.6	74.63	74.6	Al ₂ O ₃

此, 固溶时效处理后耐蚀性能得到提高。此外, SAT500 试样表面钝化膜中的 TiO₂ 含量最高, 其耐蚀性能最优, 与电化学测试结果一致。

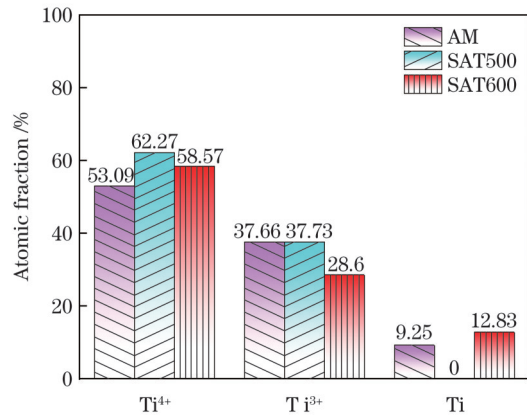


图 7 不同试样表面钝化膜中的 Ti 元素价态分布情况

Fig. 7 Valence distributions of Ti elements in passive films formed on different sample surfaces

3.3 微观组织分析

图 8 和图 9 分别显示了 AM、SAT500 和 SAT600

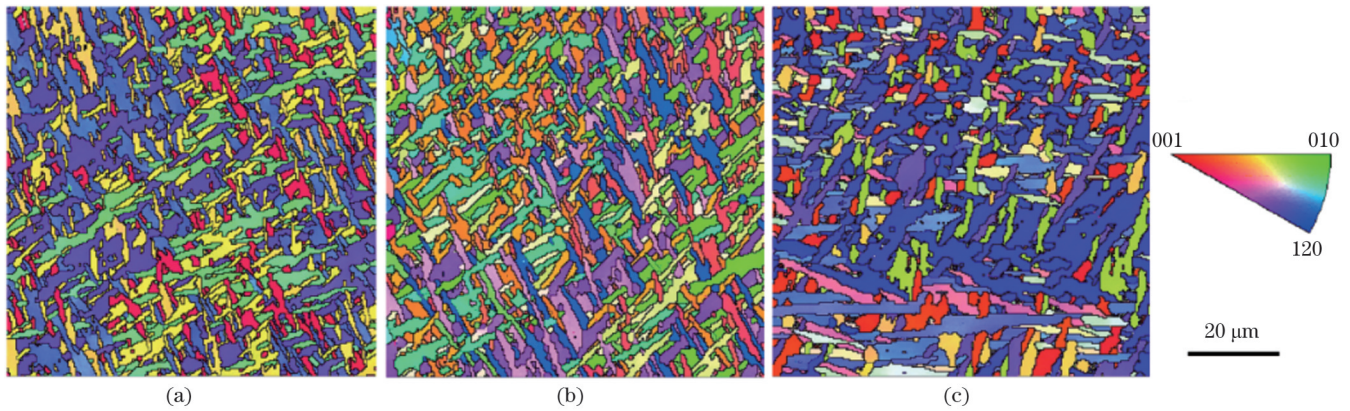


图 8 不同试样的 IPF。(a)AM;(b)SAT500;(c)SAT600

Fig. 8 IPFs of different samples. (a) AM; (b) SAT500; (c) SAT600

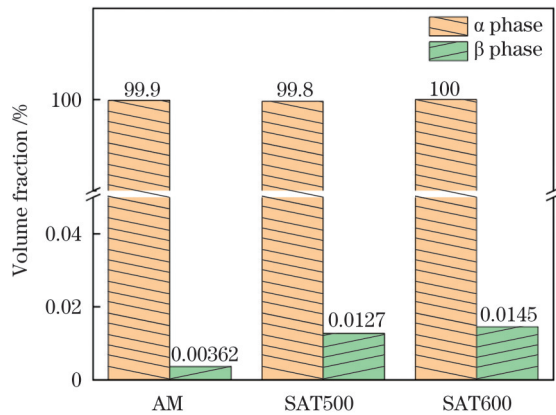


图 9 不同试样中相的分布情况

Fig. 9 Phase distributions in different samples

试样的反极图(IPF)及 α 相、 β 相的相对含量。观察发现,AM试样主要由大量针状 α' 相组成,经固溶时效处理后,针状 α' 相减少,部分转变为片状 α 相。与SAT500试样相比,SAT600试样中的 α 片层较厚。此外,固溶时效处理前试样中的 β 相含量较少,处理后有增多趋势。因为增材制造过程中激光功率密度较大,大约为 $1.43 \times 10^8 \text{ W/m}^2$,在激光强烈热作用下钛合金

经历快速熔化和凝固,再加上增材制造逐层制造的特点,后一层对前一层具有重熔作用,导致钛合金增材件内部形成大量非平衡相 α' 相和少量 β 相,呈现出典型的魏氏组织特征。经固溶时效处理后,随着V元素的扩散, α' 相转变为 α 相,同时在 α' 相边界位置形成 β 相, β 相含量增加^[22]。

图 10 显示了 AM、SAT500 和 SAT600 试样中晶粒大小的分布情况。对比发现,固溶时效处理后晶粒尺寸有粗化趋势,可能是因为时效温度较高,时间较长,故晶粒长大。图 11 显示了 AM、SAT500 和 SAT600 试样的局部取向差(KAM)结果,KAM 能反映材料内部的局部残余应力的水平和位错密度分布。观察发现,AM 试样中的残余应力较大。这是因为在激光增材制造过程中,高功率密度的激光与材料相互作用,材料经历不均匀快速熔化凝固过程,在材料内产生很大温度梯度,进而产生不均匀热应力,最终增材件内部产生较大残余应力。SAT500 和 SAT600 试样中的残余应力和位错密度较低,说明经过固溶时效热处理后,试样中的残余应力和位错密度降低。

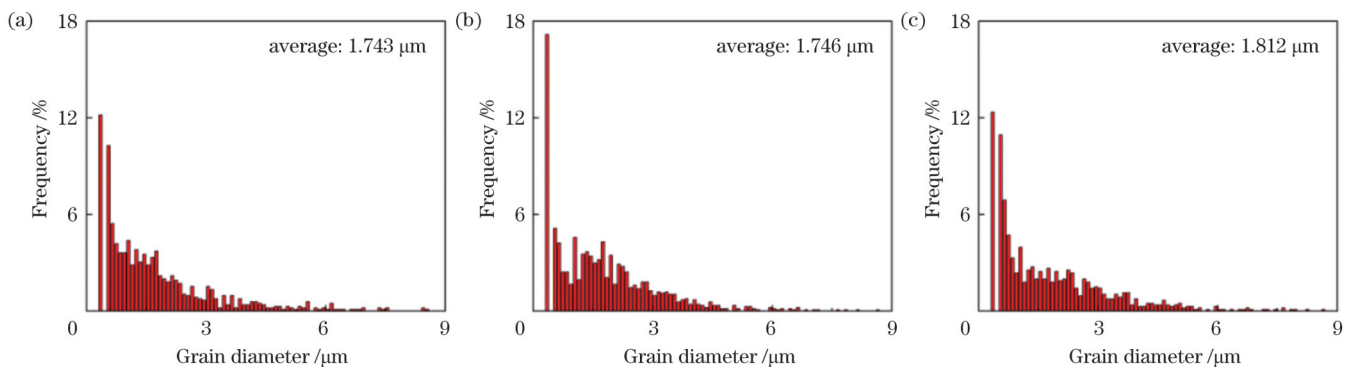


图 10 不同试样中的晶粒大小分布。(a)AM;(b)SAT500;(c)SAT600

Fig. 10 Grain size distributions in different samples. (a) AM; (b) SAT500; (c) SAT600

图 12 显示了 AM、SAT500 和 SAT600 试样中的晶界分布情况,其中LAGB表示小角度晶界,HAGB表示大角度晶界。对比发现,经过固溶时效处理后,

LAGB比例从0.343(AM试样)减小为0.203(SAT500试样)和0.105(SAT600试样)。已有研究表明,位错密度增加会促进LAGB形成^[23]。根据图 11 可知,AM

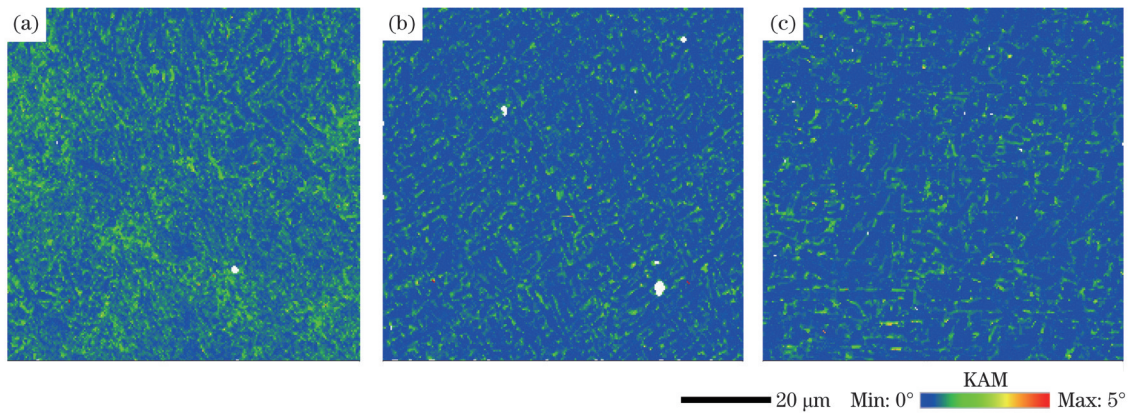


图 11 不同试样的 KAM 图。(a)AM;(b)SAT500;(c)SAT600
Fig. 11 KAM maps of different samples. (a) AM; (b) SAT500; (c) SAT600

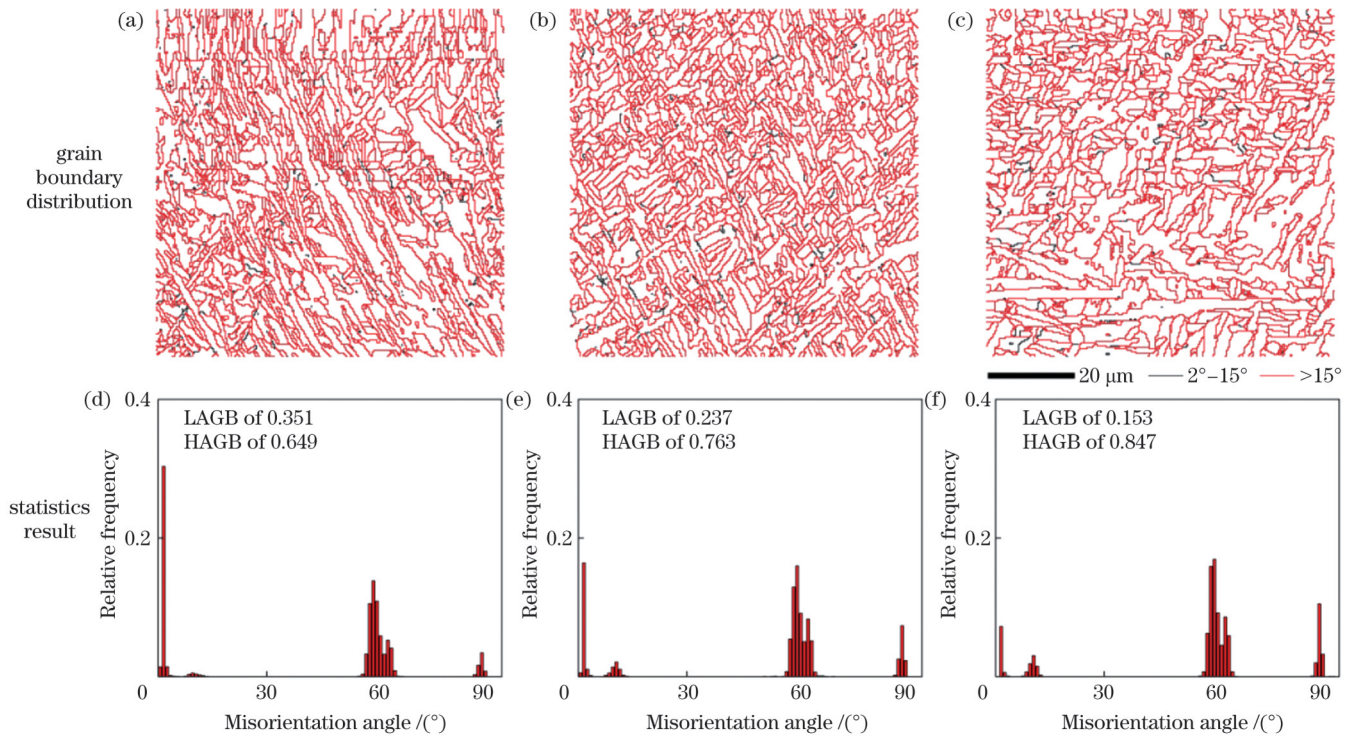


图 12 不同试样中的晶界分布和统计结果。(a)(d)AM;(b)(e)SAT500;(c)(f)SAT600
Fig. 12 Grain boundary distributions and statistics results in different samples. (a)(d) AM; (b)(e) SAT500; (c)(f) SAT600

试样的位错密度要高于 SAT500 和 SAT600 试样,因此 AM 试样中的 LAGB 比例最高。

4 讨论分析

基于电化学测试和 XPS 分析研究发现,固溶时效处理可显著改善激光熔丝真空增材 Ti6Al4V 的耐蚀性能,原因归结于固溶时效处理后材料微观组织的变化。具体表现为,固溶时效处理后试样中 β 相的含量增多, β 相的耐蚀性能优于针状 α' 相。此外, β 和 α 两相间存在电位差而引发原电池腐蚀^[24],但是固溶时效处理后 Ti6Al4V 中 β 、 α 两相的体积比降低,导致腐蚀原电池中阴极和阳极的相对面积比减小,使得腐蚀速率减缓,耐蚀性能增强^[25]。但是图 9 显示,三个试样中的 β 相含量均较少,因此推测 β 相含量对耐蚀性能的影响

较小,与已有研究结论^[26]一致。图 11 显示,固溶时效处理后位错密度显著减小,位错附近产生局部晶格畸变,具有较高的电化学活性,电化学腐蚀易在此处发生^[27],因此减小位错密度有利于增强耐蚀性能。另外,晶界对耐蚀性能有重要影响。一方面,晶界容易引起微观腐蚀,与小角度晶界相比,大角度晶界更易受到腐蚀,而固溶时效处理后大角度晶界的比例增加,导致耐蚀性能下降。但另一方面,晶界处于高能态,更易成为钝化膜形核点,加速钝化膜形成^[28],可提高耐蚀性能。综合腐蚀行为结果显示,固溶时效热处理可提高耐蚀性能,说明晶界作为形核点促进钝化膜形成的作用要大于其腐蚀的作用。与 SAT500 试样相比,SAT600 试样中的大角度晶界含量更高,但是耐蚀性比 SAT500 试样差,主要原因是 SAT600 试样中的 α 片层

变厚,耐蚀性能变差^[29]。

5 结 论

通过对固溶时效热处理前后激光熔丝真空增材制造 Ti6Al4V 钛合金的腐蚀行为和微观组织进行对比研究,得出以下结论:

1) 固溶时效热处理可减缓腐蚀速率,增强耐蚀性能。与 SAT500 试样相比,SAT600 试样的 α 片层变厚,导致耐蚀性能变差。

2) 固溶时效热处理后,试样表面钝化膜中的 TiO_2 含量明显增多,且钝化膜更稳定,导致耐蚀性能增强。

3) 固溶时效热处理后试样中的针状 α' 相减少,大角度晶界比例增加,导致耐蚀性能增强。

参 考 文 献

- [1] Nguyen H D, Pramanik A, Basak A K, et al. A critical review on additive manufacturing of Ti-6Al-4V alloy: microstructure and mechanical properties[J]. *Journal of Materials Research and Technology*, 2022, 18: 4641-4661.
- [2] Attar H, Calin M, Zhang L C, et al. Manufacture by selective laser melting and mechanical behavior of commercially pure titanium[J]. *Materials Science and Engineering: A*, 2014, 593: 170-177.
- [3] Gibson B T, Bandari Y K, Richardson B S, et al. Melt pool size control through multiple closed-loop modalities in laser-wire directed energy deposition of Ti-6Al-4V[J]. *Additive Manufacturing*, 2020, 32: 100993.
- [4] Liu S, Brice C, Zhang X L. Interrelated process-geometry-microstructure relationships for wire-feed laser additive manufacturing [J]. *Materials Today Communications*, 2022, 31: 103794.
- [5] Fu Y L, Demir A G, Guo N. Additive manufacturing of Ti-6Al-4V alloy by micro-laser metal wire deposition with pulsed wave emission: processability and microstructure formation[J]. *The International Journal of Advanced Manufacturing Technology*, 2023, 126(5): 2693-2711.
- [6] Sun W Z, Shan F H, Zong N F, et al. A simulation and experiment study on phase transformations of Ti-6Al-4V in wire laser additive manufacturing[J]. *Materials & Design*, 2021, 207: 109843.
- [7] Brandl E, Palm F, Michailov V, et al. Mechanical properties of additive manufactured titanium (Ti-6Al-4V) blocks deposited by a solid-state laser and wire[J]. *Materials & Design*, 2011, 32(10): 4665-4675.
- [8] Mahamood R M, Akinlabi E T. Corrosion behavior of laser additive manufactured titanium alloy[J]. *The International Journal of Advanced Manufacturing Technology*, 2018, 99(5): 1545-1552.
- [9] Ibrahim M Z, Sarhan A A D, Shaikh M O, et al. Investigate the effects of the laser cladding parameters on the microstructure, phases formation, mechanical and corrosion properties of metallic glasses coatings for biomedical implant application[M]//Almangour B. *Additive manufacturing of emerging materials*. Cham: Springer, 2019: 299-323.
- [10] Yao J H, Wang Y, Wu G L, et al. Growth characteristics and properties of micro-arc oxidation coating on SLM-produced TC4 alloy for biomedical applications[J]. *Applied Surface Science*, 2019, 479: 727-737.
- [11] Ramasamy P, Sundharam S. Microhardness and corrosion resistance of plasma sprayed bioceramic bilayer coated Ti-6Al-4V implants[J]. *Journal of the Australian Ceramic Society*, 2021, 57(2): 605-613.
- [12] Li J Q, Lin X, Wang J, et al. Effect of stress-relief annealing on anodic dissolution behaviour of additive manufactured Ti-6Al-4V via laser solid forming[J]. *Corrosion Science*, 2019, 153: 314-326.
- [13] Etefagh A H, Zeng C Y, Guo S M, et al. Corrosion behavior of additively manufactured Ti-6Al-4V parts and the effect of post annealing[J]. *Additive Manufacturing*, 2019, 28: 252-258.
- [14] Xu Y Z, Lu Y, Sundberg K L, et al. Effect of annealing treatments on the microstructure, mechanical properties and corrosion behavior of direct metal laser sintered Ti-6Al-4V[J]. *Journal of Materials Engineering and Performance*, 2017, 26(6): 2572-2582.
- [15] 窦恩惠, 肖美立, 柯林达, 等. 热处理对激光选区熔化成形 TC11 钛合金组织性能的影响[J]. *中国激光*, 2021, 48(6): 0602117.
- [16] Dou E H, Xiao M L, Ke L D, et al. Effect of heat treatment on microstructure and mechanical properties of selective-laser-melted TC11 titanium alloys[J]. *Chinese Journal of Lasers*, 2021, 48(6): 0602117.
- [17] Liu Z, Zhao Z B, Liu J R, et al. Effects of solution-aging treatments on microstructure features, mechanical properties and damage behaviors of additive manufactured Ti-6Al-4V alloy[J]. *Materials Science and Engineering: A*, 2021, 800: 140380.
- [18] Su J L, Xie H M, Tan C L, et al. Microstructural characteristics and tribological behavior of an additively manufactured Ti-6Al-4V alloy under direct aging and solution-aging treatments[J]. *Tribology International*, 2022, 175: 107763.
- [19] 王普强, 王豫跃, 吴梦杰, 等. 热处理对 LMD TC4 组织、力学性能及各向异性的影响[J]. *中国激光*, 2021, 48(10): 1002116.
- [20] Wang P Q, Wang Y Y, Wu M J, et al. Effects of heat treatment on microstructure, mechanical properties, and anisotropy of laser melting deposited TC4[J]. *Chinese Journal of Lasers*, 2021, 48(10): 1002116.
- [21] Caballero A, Ding J L, Bandari Y, et al. Oxidation of Ti-6Al-4V during wire and arc additive manufacture[J]. *3D Printing and Additive Manufacturing*, 2019, 6(2): 91-98.
- [22] Bermingham M J, Thomson-Larkins J, St John D H, et al. Sensitivity of Ti-6Al-4V components to oxidation during out of chamber Wire + Arc Additive Manufacturing[J]. *Journal of Materials Processing Technology*, 2018, 258: 29-37.
- [23] Ding W W, Wang Z W, Chen G, et al. Oxidation behavior of low-cost CP-Ti powders for additive manufacturing via fluidization[J]. *Corrosion Science*, 2021, 178: 109080.
- [24] Sallica-Leva E, Caram R, Jardini A L, et al. Ductility improvement due to martensite α' decomposition in porous Ti-6Al-4V parts produced by selective laser melting for orthopedic implants [J]. *Journal of the Mechanical Behavior of Biomedical Materials*, 2016, 54: 149-158.
- [25] Hanawa T, Asami K, Asaoka K. Repassivation of titanium and surface oxide film regenerated in simulated bioliquid[J]. *Journal of Biomedical Materials Research*, 1998, 40(4): 530-538.
- [26] Wu B T, Pan Z X, Li S Y, et al. The anisotropic corrosion behaviour of wire arc additive manufactured Ti-6Al-4V alloy in 3.5% NaCl solution[J]. *Corrosion Science*, 2018, 137: 176-183.
- [27] Xu Y, Li Z P, Zhang G Q, et al. Electrochemical corrosion and anisotropic tribological properties of bioinspired hierarchical morphologies on Ti-6Al-4V fabricated by laser texturing[J]. *Tribology International*, 2019, 134: 352-364.
- [28] Metikoš-Huković M, Kwokal A, Piljac J. The influence of niobium and vanadium on passivity of titanium-based implants in physiological solution[J]. *Biomaterials*, 2003, 24(21): 3765-3775.
- [29] 王占栋, 王世彬, 吴二柯, 等. 水下定向能量沉积修复钛合金电化学腐蚀特性研究[J]. *中国激光*, 2022, 49(14): 1402806.
- [30] Wang Z D, Wang S B, Wu E K, et al. Study on electrochemical corrosion characteristics of titanium alloy repaired by underwater directional energy deposition[J]. *Chinese Journal of Lasers*, 2022, 49(14): 1402806.
- [31] Gong X J, Cui Y J, Wei D X, et al. Building direction dependence of corrosion resistance property of Ti-6Al-4V alloy fabricated by electron beam melting[J]. *Corrosion Science*, 2017, 127: 101-109.
- [32] Dai N W, Zhang L C, Zhang J X, et al. Distinction in corrosion resistance of selective laser melted Ti-6Al-4V alloy on different planes[J]. *Corrosion Science*, 2016, 111: 703-710.

Effect of Solution-Aging Treatment on Corrosion Resistance of Ti6Al4V via Laser Wire Vacuum Additive Manufacturing

Ding Xueping^{1*}, Zhang Qi², Ma Honglin²

¹*School of Material Science and Engineering, Chongqing University of Technology, Chongqing 400054, China;*

²*Chongqing Key Laboratory of Additive Manufacturing Technology and Systems, Chongqing Institute of Green and Intelligent Technology, Chinese Academy of Sciences, Chongqing 400714, China*

Abstract

Objective Laser wire vacuum additive manufacturing (LWVAM) is a highly promising metallic additive manufacturing technology. However, Ti6Al4V alloys fabricated via LWVAM have inferior corrosion resistance due to the higher fraction of acicular α' phase and larger residual stress from rapid melting and solidification in the laser additive manufacturing process. Previous studies have shown that annealing treatment can improve corrosion resistance in Ti6Al4V parts fabricated by laser additive manufacturing, but their strength and hardness are reduced. As is known, solution-aging treatment (SAT) can not only improve the strength and hardness of titanium alloy, but also its ductility and toughness. Therefore, this study investigates the effect of solution-aging treatment on the corrosion resistance of Ti6Al4V via laser wire vacuum additive manufacturing to explain the underlying reasons for the changes in corrosion resistance based on microstructure analysis.

Methods Ti6Al4V samples are fabricated by laser wire vacuum additive manufacturing. The solution-aging treatment parameters are shown in Table 1. To simplify the description, the as-fabricated sample and solution-aging treatment samples are labeled AM, SAT500 and SAT600, respectively. The microstructure of samples is observed by scanning electron microscope (SEM) with electron back-scatter diffraction (EBSD). The electrochemical tests, including electrochemical impedance spectroscopy (EIS) and potentiodynamic polarization, are conducted in NaCl water solution with mass fraction of 3.5%. An X-Ray photoelectron spectroscopy (XPS) surface analysis system is used to analyze the elemental composition and valence state of the passive film.

Results and Discussions The potentiodynamic polarization results show that the corrosion current density value of the AM sample is about 74.83 times and 7.39 times higher than that of the SAT500 and SAT samples, respectively, indicating that SAT is conducive to improving the corrosion resistance of the sample fabricated by LWVAM. Compared to the SAT600 sample, the SAT500 sample has better corrosion resistance. These conclusions are also borne out by EIS test results. XPS results show that the intensity of TiO_2 is much stronger than that of Ti_2O_3 and TiO , suggesting that TiO_2 is the primary component in the passive film. In addition, it is found that in solution-aging treatment samples, there is more TiO_2 than in the AM sample (Fig. 5). Previous studies showed that high-valence oxides had stabler and better protection. Therefore, solution-aging treatment is helpful to obtain better corrosion resistance. The SAT500 sample has the highest TiO_2 content, indicating that the SAT500 sample has the best corrosion resistance. EBSD results show that after solution-aging treatment, the acicular α' phase in the AM sample changes to the lamellar α phase. Compared to the SAT500 sample, the α lath is coarser for the SAT600 sample (Fig. 6). It is also suggested that after solution-aging treatment, local misorientation is significantly reduced and the dislocation density and residual stress decrease significantly (Fig. 9). In addition, it is found that the number fraction of low angle grain boundary (corresponding to the misorientation angle of 2° – 15°) decreases from 0.343 (AM sample) to 0.203 (SAT500 sample) and 0.105 (SAT600 sample) (Fig. 10). As is known, acicular α' phase is a high energy phase with inferior corrosion resistance. After solution-aging treatment, the decrease of α' phase is thus beneficial to improve the corrosion resistance. In addition, the dislocation density is prone to corrosion due to the high activation energy. The decrease of dislocation density is thus useful to enhance the corrosion resistance due to the solution-aging treatment. Moreover, it has been suggested that grain boundaries are prone to corrosion due to higher lattice distortion than in the grain interior. Furthermore, the high angle grain boundary energy is higher than that of the low angle grain boundary. The high angle grain boundaries are more vulnerable to corrosive solution attack. In fact, owing to the higher energy, grain boundaries are preferential sites for the nucleation of protective layers. Therefore, a higher number fraction of high grain boundary is found in the solution-aging treatment sample with better corrosion resistance. In addition, it is found that in the SAT600 sample, the α lath is coarser than in the SAT500 sample, leading to the inferior corrosion resistance of the SAT600 sample.

Conclusions In the present study, the effect of solution-aging treatment on the corrosion resistance of Ti6Al4V via laser wire vacuum additive manufacturing is investigated. Results show that after solution-aging treatment, the corrosion current density of the samples decreases and the passive film formed on the solution-aging treatment sample consists of more high-valence oxide TiO_2 , which has stabler and better protection. The reason is due to less acicular α' phase and more high angle grain boundary in solution-aging treatment samples, showing solution-aging treatment to be conducive to improving corrosion resistance. Moreover, compared with the SAT500 sample, the α lath is coarser in the SAT600 sample, leading to inferior corrosion resistance.

Key words laser technique; laser vacuum additive manufacturing; Ti6Al4V alloy; solution-aging treatment; corrosion resistance